Electronic Supplementary Information (ESI) for

A dynamic, luminescent and entangled MOF as a qualitative sensor for volatile organic solvents and quantitative monitor for acetonitrile vapour

Jun-Hao Wang, Mian Li and Dan Li*

Department of Chemistry and Research Institute for Biomedical and Advanced Materials,

Shantou University, Guangdong 515063, P. R. China.

E-mail: dli@stu.edu.cn

Supplementary Index

Experimental Section

Synthetic details of 2,6-bis((3,5-dimethyl-1*H*-pyrazol-4-yl)methyl)pyridine: The ligand was synthesized according to the procedure as described previously[1] with a little modification. Sodium acetylacetonate (2.45 g, 20 mmol) was added to a stirred, refluxing *t*-butyl alcohol (80 mL). After 5 min, 2,6-bis-(bromomethyl)-pyridine (2.65 g, 10 mmol) was added during a 10-min period. 30 min after the addition, 0.5 g of KI and 0.2 g of 15-crown-5 were added. The reaction mixture was stirred and heated at reflux temperature for about 10 hours. After three-fourths of the solvent was distilled, the solid residue was washed thoroughly with water and extracted with dichloromethane. The extracts were dried over anhydrous Na_2SO_4 and the solvent was distilled. The residual oil was dissolved in 60 mL ethanol, and excess hydrazine hydrate was added to the solution. The solution was stirred and heated under refluxing temperature for 5 hours. After the solution was concentrated, large amount of water was added. The resultant white solid was filtered off, washed with water and dried (1.78 g, yield ca. 60 %). ^{1}H-NMR (CD_3OD, 400MHz): δ = 7.55 (1H, t, PyH, J = 7.7Hz), 6.84 (2H, d, PyH), 3.88 (4H, s, Py-CH_2-Pz), 2.09 (12H, s, Pz-CH_3).

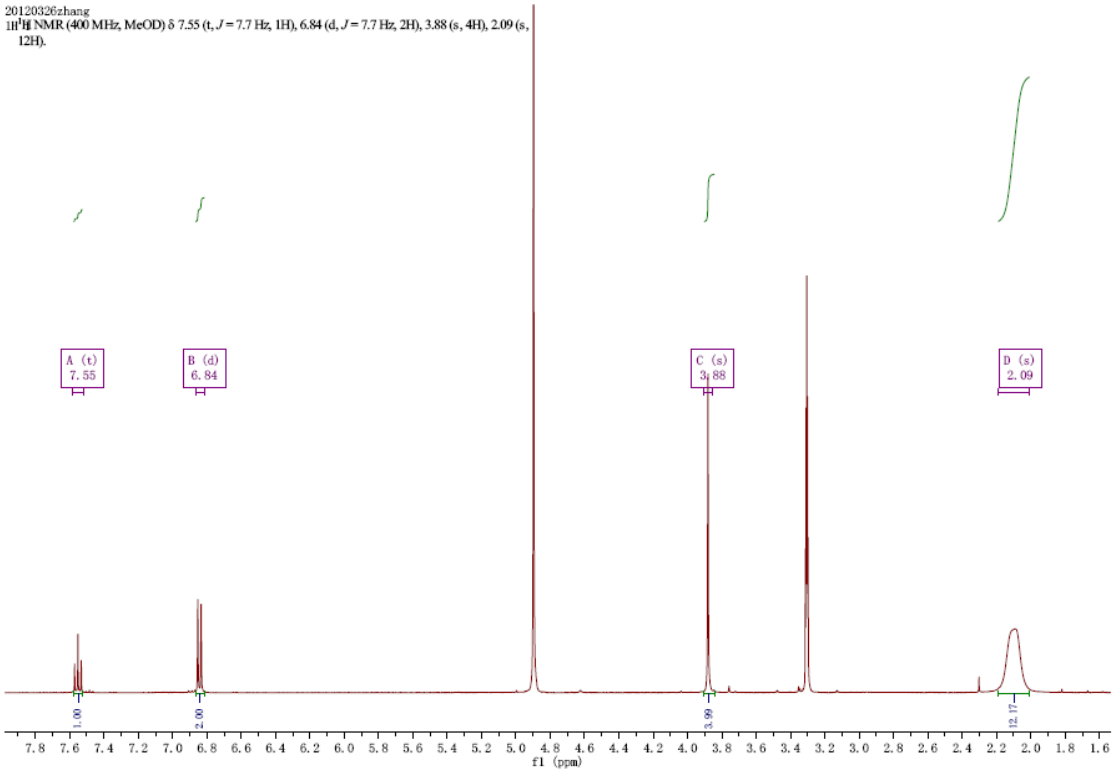

Fig. S1. ^{1}H-NMR of 2,6-bis((3,5-dimethyl-1*H*-pyrazol-4-yl)methyl)pyridine.

[1] G.-F. Gao, M. Li, S.-Z. Zhan, Z. Lv, G.-h. Chen and D. Li, *Chem. Eur. J.*, 2011, **17**, 4113-4117.

Crystal Data Section

Table S1. Summary of the Crystal Data and Structure Refinement Parameters

Parameters	**1·$C_2H_5OH·H_2O$ (298K)**	**1·$C_2H_5OH·H_2O$ (100K)**	**1·C_6H_6 (298K)**	**1·C_6H_{12} (298K)**	**1·MeCN·H_2O (298K)**	**1·MeCN·H_2O (100K)**	**1·THF·H_2O (298K)**
Formula	$C_{22}H_{29}Cu_3N_8O_2$	$C_{22}H_{29}Cu_3N_8O_2$	$C_{26}H_{27}Cu_3N_8$	$C_{26}H_{23}Cu_3N_8$	$C_{22}H_{26}Cu_3N_9O$	$C_{22}H_{26}Cu_3N_9O$	$C_{24}H_{31}Cu_3N_8O_2$
M_r	628.13	628.13	642.18	648.22	623.14	623.14	654.17
Temp (*K*)	298	100	298	298	298	100	298
Space group	*P*-1	*P-1*	*P*-1	*P*-1	*P*-1	*P-1*	*P*-1
a (Å)	11.4964	11.5152	11.4287	11.4507	11.4262	11.3700	11.4723
b (Å)	11.3571	11.3120	11.7031	11.6026	11.4509	11.4274	11.4569
c (Å)	12.9352	12.6953	12.918	13.2025	12.5243	12.1912	13.1199
α (deg)	115.386	114.171	64.005	65.360	66.620	67.952	64.295
β (deg)	91.133	91.497	89.783	71.368	89.182	87.743	89.824
γ (deg)	69.305	68.347	71.129	71.461	69.908	69.803	110.147
V(Å^3)	1404.8	1386.9	1450.1	1475.61	1398.38	1370.45	1434.82
Z	2	2	2	2	2	2	2
D_{calcd}(g cm^{-3})	1.472	1.497	1.471	1.459	1.340	1.505	1.510
μ (mm^{-1})	2.274	2.312	2.208	2.171	2.804	2.337	2.238
Reflcns collcd	9916	9785	8472	10464	9078	9451	10456
Unique reflcns	4981	4889	5028	5185	5390	4837	5056
R_{int}	0.0206	0.0170	0.0297	0.0359	0.0311	0.0263	0.0219
R1[I>2σ(I)][a]	0.0352	0.0371	0.0641	0.0464	0.0621	0.0571	0.0372
*w*R2[I>2σ(I)][a]	0.1096	0.1306	0.1575	0.1083	0.1940	0.1896	0.1030
R1(all data)	0.0483	0.0420	0.0880	0.0787	0.0793	0.0691	0.0501
*w*R2(all data)	0.1258	0.1364	0.1868	0.1263	0.2170	0.2084	0.1144
GOOF	0.892	1.101	1.025	1.020	1.042	1.058	1.037

[a] $R_1=\sum(||F_0|-|F_c||)/\sum|F_0|$; $wR_2=[\sum_w(F_0^2-F_c^2)^2/\sum w(F_0^2)^2]^{1/2}$

Table S2. Selected Bond Lengths (Å) and Bond Angles (°)

$1{\cdot}C_2H_5OH{\cdot}H_2O$ (298K)			
Cu(1)-C(20)#3	1.8623(17)	C(20)#3-Cu(1)-N(6)	134.25(9)
Cu(1)-N(6)	1.9302(14)	C(20)#3-Cu(1)-N(5)	124.24(8)
Cu(1)-N(5)	2.0131(17)	N(6)-Cu(1)-N(5)	101.49(7)
Cu(2)-C(18)	1.8603(17)	C(18)-Cu(2)-N(1)#1	136.91(8)
Cu(2)-N(1)#1	1.9853(14)	C(18)-Cu(2)-N(7)	121.81(8)
Cu(2)-N(7)	2.0044(17)	N(1)#1-Cu(2)-N(7)	98.55(6)
Cu(2)-Cu(2)#2	2.8504(5)	C(19)-Cu(3)-N(8)	134.20(7)
Cu(3)-C(19)	1.8733(18)	C(19)-Cu(3)-N(3)#6	121.60(6)
Cu(3)-N(8)	1.9101(16)	N(8)-Cu(3)-N(3)#6	104.14(6)
Cu(3)-N(3)#6	2.0711(13)	C(11)-C(12)-C(15)	115.46(17)
		C(3)-C(6)-C(7)	116.03(17)
Symmetry codes: #1 x-1,y,z+1 #2 -x+2,-y,-z #3 x,y-1,z-1 #6 x,y,z+1			
$1{\cdot}C_2H_5OH{\cdot}H_2O$ (100K)			
Cu(1)-C(20)#1	1.867(2)	C(20)#1-Cu(1)-N(6)	134.61(10)
Cu(1)-N(6)	1.9188(17)	C(20)#1-Cu(1)-N(5)	123.56(9)
Cu(1)-N(5)	2.009(2)	N(6)-Cu(1)-N(5)	101.82(8)
Cu(2)-C(18)	1.870(2)	C(18)-Cu(2)-N(1)#3	136.55(8)
Cu(2)-N(1)#3	1.9781(16)	C(18)-Cu(2)-N(7)	120.64(9)
Cu(2)-N(7)	1.9928(19)	N(1)#3-Cu(2)-N(7)	98.92(7)
Cu(2)-Cu(2)#4	2.7524(5)	C(19)-Cu(3)-N(8)	135.82(8)
Cu(3)-C(19)	1.867(2)	C(19)-Cu(3)-N(3)#5	120.51(8)
Cu(3)-N(8)	1.9138(19)	N(8)-Cu(3)-N(3)#5	103.48(8)
Cu(3)-N(3)#5	2.0622(17)	C(3)-C(6)-C(7)	115.77(19)
		C(15)-C(12)-C(11)	115.3(2)
Symmetry codes: #1 x,y-1,z-1 #2 x+1,y,z-1 #3 x-1,y,z+1 #4 -x+2,-y,-z #5 x,y,z+1			

(Continued)

1·C_6H_6 (298K)			
Cu(1)-C(20)#1	1.837(7)	C(20)#1-Cu(1)-N(6)	133.8(3)
Cu(1)-N(6)	1.933(6)	C(20)#1-Cu(1)-N(5)	128.7(3)
Cu(1)-N(5)	2.017(5)	N(6)-Cu(1)-N(5)	97.5(2)
Cu(2)-C(18)	1.865(7)	C(18)-Cu(2)-N(7)	126.5(2)
Cu(2)-N(7)	1.980(6)	C(18)-Cu(2)-N(1)#3	135.0(2)
Cu(2)-N(1)#3	1.996(5)	N(7)-Cu(2)-N(1)#3	97.3(2)
Cu(2)-Cu(2)#4	2.9346(18)	C(19)-Cu(3)-N(8)	134.0(3)
Cu(3)-C(19)	1.852(6)	C(19)-Cu(3)-N(3)#5	121.8(2)
Cu(3)-N(8)	1.898(6)	N(8)-Cu(3)-N(3)#5	104.2(2)
Cu(3)-N(3)#5	2.067(4)	C(7)-C(6)-C(3)	115.8(5)
		C(11)-C(12)-C(15)	115.4(5)
Symmetry codes: #1 x,y+1,z-1 #2 x-1,y,z-1 #3 x+1,y,z+1 #4 -x+1,-y+2,-z+1 #5 x,y,z+1			
1·C_6H_{12} (298K)			
Cu(1)-C(20)#2	1.851(6)	C(20)#2-Cu(1)-N(6)	136.3(2)
Cu(1)-N(6)	1.933(5)	C(20)#2-Cu(1)-N(5)	125.9(2)
Cu(1)-N(5)	2.030(4)	N(6)-Cu(1)-N(5)	97.85(17)
Cu(2)-C(18)	1.867(6)	C(18)-Cu(2)-N(7)	130.96(18)
Cu(2)-N(7)	1.969(4)	C(18)-Cu(2)-N(1)#3	131.70(19)
Cu(2)-N(1)#3	2.008(4)	N(7)-Cu(2)-N(1)#3	96.71(17)
Cu(2)-Cu(2)#4	3.0599(13)	C(19)-Cu(3)-N(8)	133.14(18)
Cu(3)-C(19)	1.864(5)	C(19)-Cu(3)-N(3)#6	123.55(17)
Cu(3)-N(8)	1.921(5)	N(8)-Cu(3)-N(3)#6	103.29(16)
Cu(3)-N(3)#6	2.079(3)	C(7)-C(6)-C(3)	115.4(4)
		C(11)-C(12)-C(15)	115.5(4)
Symmetry codes: #1 x+1,y+1,z-1 #2 x,y,z-1 #3 x-1,y-1,z+1 #4 -x-1,-y-2,-z+1 #5 x,y+1,z-1 #6 x,y-1,z+1			

(Continued)

1·THF·H_2O (298K)			
Cu(1)-C(20)#2	1.8596(17)	C(20)#2-Cu(1)-N(6)	135.46(9)
Cu(1)-N(6)	1.9283(14)	C(20)#2-Cu(1)-N(5)	124.70(8)
Cu(1)-N(5)	2.0244(18)	N(6)-Cu(1)-N(5)	99.84(7)
Cu(2)-C(18)	1.8668(17)	C(18)-Cu(2)-N(7)	126.07(9)
Cu(2)-N(7)	1.9808(17)	C(18)-Cu(2)-N(1)#3	134.42(8)
Cu(2)-N(1)#3	1.9933(16)	N(7)-Cu(2)-N(1)#3	97.97(6)
Cu(2)-Cu(2)#4	2.9342(6)	C(19)-Cu(3)-N(8)	134.29(8)
Cu(3)-C(19)	1.872(2)	C(19)-Cu(3)-N(3)#6	122.02(6)
Cu(3)-N(8)	1.9171(15)	N(8)-Cu(3)-N(3)#6	103.67(7)
Cu(3)-N(3)#6	2.0694(15)	C(3)-C(6)-C(7)	115.75(18)
		C(15)-C(12)-C(11)	115.56(19)
Symmetry codes: #1 x+1,y,z-1 #2 x,y+1,z-1 #3 x-1,y,z+1 #4 -x,-y+2,-z+2 #5 x,y,z-1 #6 x,y,z+1			
1·MeCN·H_2O (298K)			
Cu(1)-C(20)#1	1.863(5)	C(20)#1-Cu(1)-N(6)	136.7(2)
Cu(1)-N(6)	1.928(5)	C(20)#1-Cu(1)-N(5)	125.2(2)
Cu(1)-N(5)	2.019(4)	N(6)-Cu(1)-N(5)	98.10(19)
Cu(2)-C(18)	1.861(5)	C(18)-Cu(2)-N(1)#3	134.8(2)
Cu(2)-N(1)#3	1.986(4)	C(18)-Cu(2)-N(7)	125.3(2)
Cu(2)-N(7)	1.997(5)	N(1)#3-Cu(2)-N(7)	97.8(2)
Cu(2)-Cu(2)#4	2.9080(18)	C(19)-Cu(3)-N(8)	135.5(2)
Cu(3)-C(19)	1.860(5)	C(19)-Cu(3)-N(3)#6	120.0(2)
Cu(3)-N(8)	1.921(5)	N(8)-Cu(3)-N(3)#6	104.4(2)
Cu(3)-N(3)#6	2.064(4)	C(3)-C(6)-C(7)	114.3(5)
		C(15)-C(12)-C(11)	114.7(5)
Symmetry codes: #1 x,y-1,z+1 #2 x+1,y,z+1 #3 x-1,y,z-1 #4 -x,-y+2,-z-1 #5 x,y,z+1 #6 x,y,z-1			

(Continued)

1·MeCN·H_2O (100K)			
Cu(1)-C(20)#3	1.871(6)	C(20)#3-Cu(1)-N(6)	136.0(2)
Cu(1)-N(6)	1.938(5)	C(20)#3-Cu(1)-N(5)	125.7(2)
Cu(1)-N(5)	2.014(4)	N(6)-Cu(1)-N(5)	98.2(2)
Cu(2)-C(18)	1.870(5)	C(18)-Cu(2)-N(7)	123.7(2)
Cu(2)-N(7)	1.987(5)	C(18)-Cu(2)-N(1)#4	135.2(2)
Cu(2)-N(1)#4	1.994(5)	N(7)-Cu(2)-N(1)#4	97.8(2)
Cu(2)-Cu(2)#5	2.7549(13)	C(19)-Cu(3)-N(8)	136.0(2)
Cu(3)-C(19)	1.866(6)	C(19)-Cu(3)-N(3)#1	118.1(2)
Cu(3)-N(8)	1.906(5)	N(8)-Cu(3)-N(3)#1	105.8(2)
Cu(3)-N(3)#1	2.059(5)	C(3)-C(6)-C(7)	116.3(6)
		C(15)-C(12)-C(11)	115.3(6)
Symmetry codes: #1 x,y,z-1 #2 x+1,y,z+1 #3 x,y-1,z+1 #4 x-1,y,z-1 #5 -x+1,-y,-z			

Note: Highlighted in red are short Cu···Cu contacts in the frameworks.

Structural Description Section

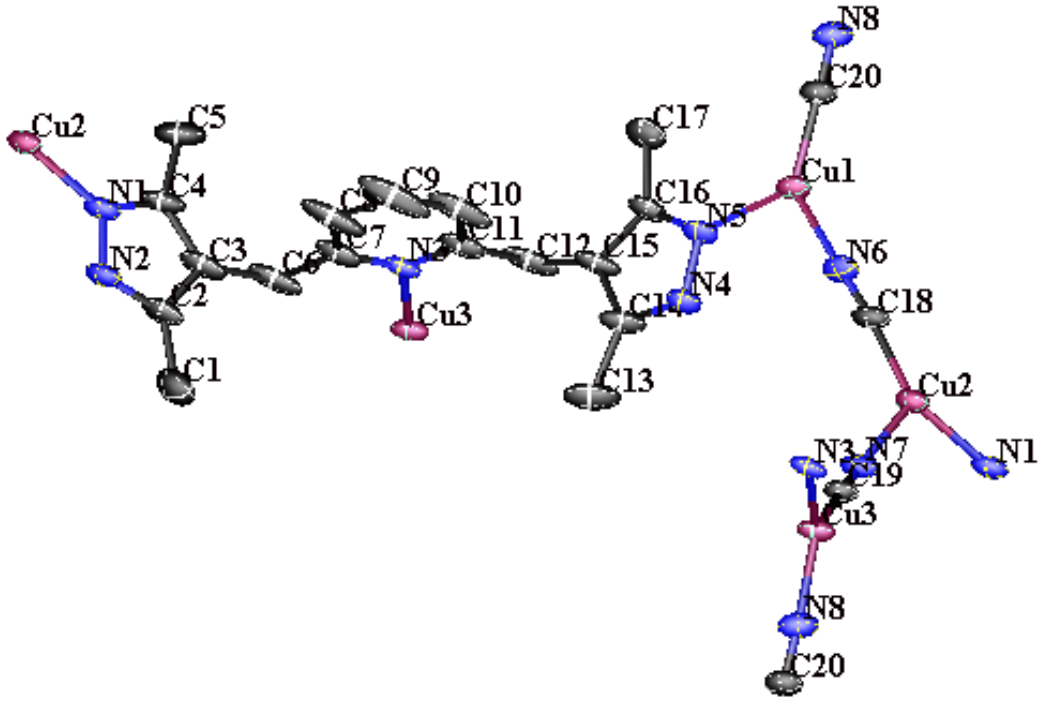

(a)

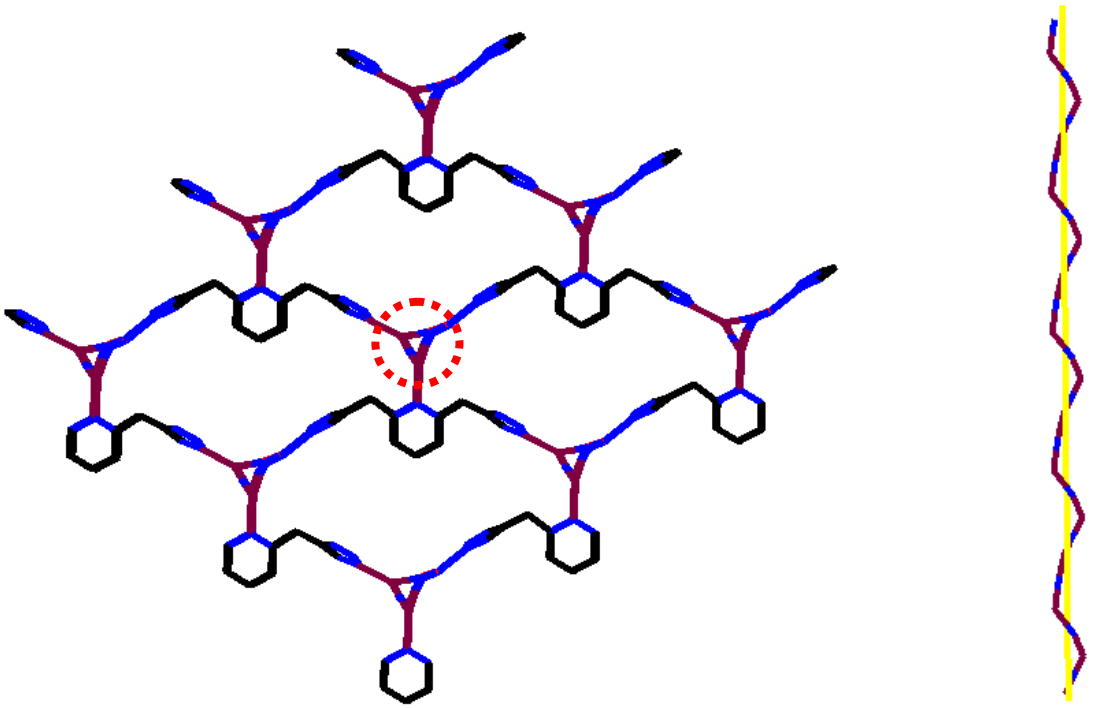

(b)

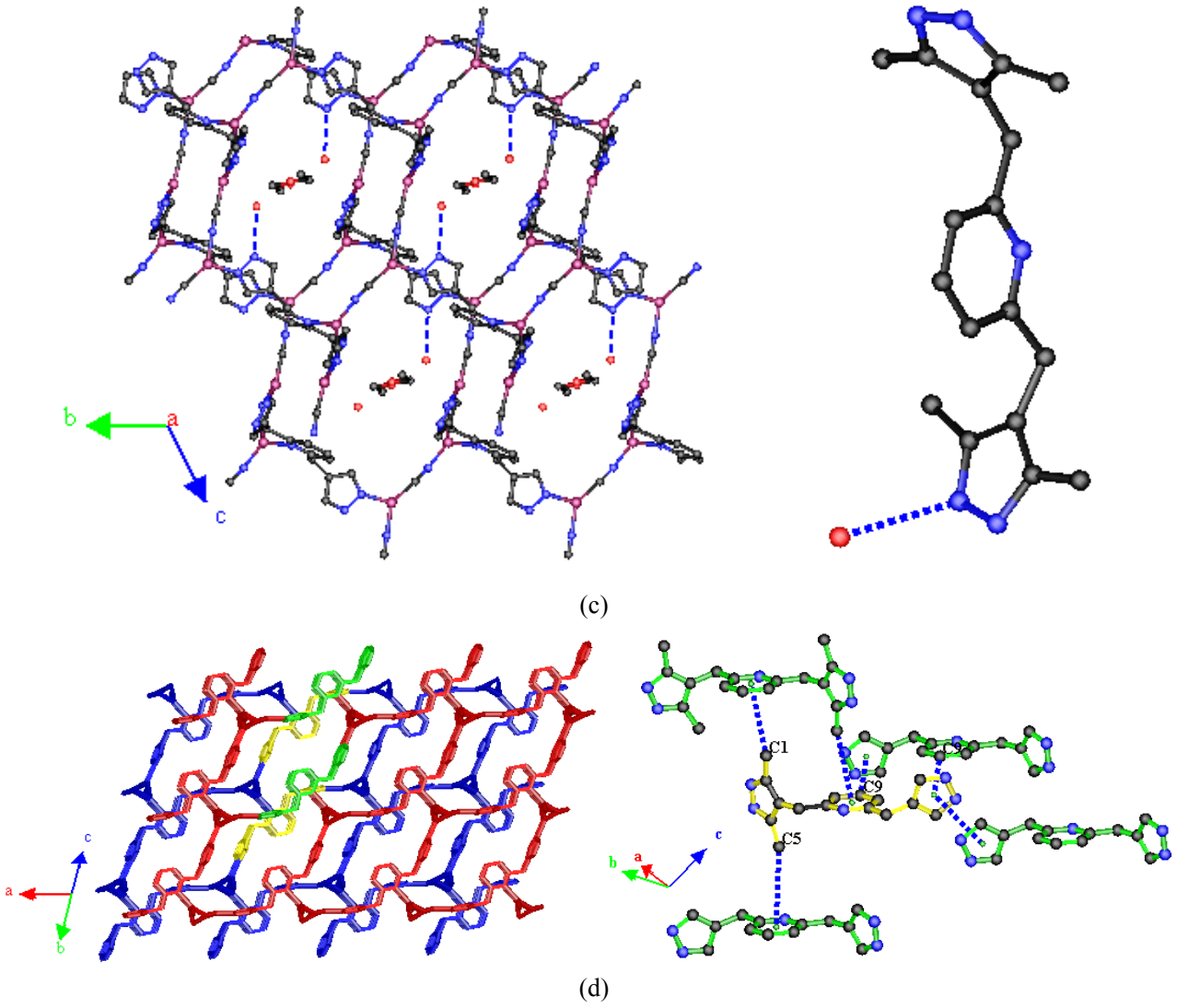

Fig. S2. Structural representations of **1**·H_2O·CH_3CH_2OH. (a) Coordination environment of the host framework of **1**. (b) A view of one single net from the CuCN chain direction (left) and the 1-D helix CuCN chain (right). (c) Two interweaving frameworks showing the accessible channels, with guest ethanol and water molecules filled in the channels (left) and the H-bond (d $_{O\text{-}N}$ = 2.9407 Å) between water guest and the N-H motif of pyrazole (right, host-guest interaction). (d) Analysis of existing weak interactions between the ligands in the host framework (host-host interaction): weak C–H···π interactions (4.0563 Å and 4.2342 Å) between methyl in the pyrazole ring; strong edge-to-face π-π interactions (3.6321 Å) between the C atoms in pyridine and the centre of pyrazole; weak face-to-face π-π interactions (4.2946Å) between pyrazole rings.

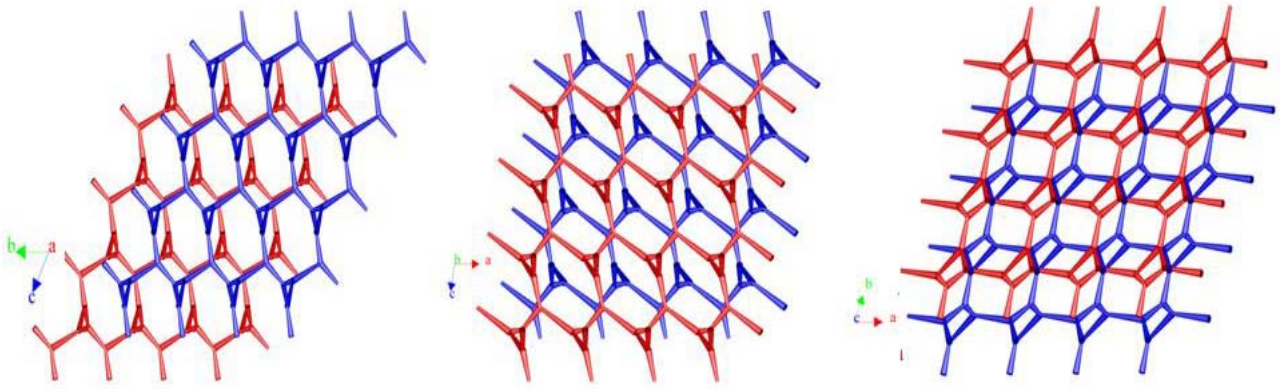

Fig. S3. Underlying net representations of the interpenetration modes of the **srs** net for the host frameworks. The window sizes of the channels: 5.4742 Å × 7.5630 Å for **1**·C_6H_6; 6.8631 Å × 7.2615 Å for **1**·THF·H_2O; 7.0550 Å × 6.9831 Å for **1**·H_2O·CH_3CH_2OH; 5.9939 Å × 6.7119 Å for **1**·MeCN·H_2O; 6.6188 Å × 7.8054 Å for **1**·C_6H_{12}. The void volume of the hosts accessible to solvents calculated by *Platon*: 28.3 % for **1**·C_6H_6; 28.9 % for **1**·THF·H_2O; 24.9% for **1**·H_2O·CH_3CH_2OH; 25.4 % for **1**·MeCN·H_2O; 30.8 % for **1**·C_6H_{12}.

Topological report concerning the entanglement of host 1:

By taking into consideration of the short Cu···Cu interactions, a new binodal SINGLE net arise, which is self-catenated and of the rare kind of nets with collision. Topological analysis report of TOPOS is given below.

Point symbol for net: {8^2.10}3{8^3.10^3}

3,4-c net with stoichiometry (3-c)3(4-c); 2-nodal net

VS [8.8.10(6)][8(2).10(5).8(2).10(5).8(2).10(5)]

WARNING (STRUCTURE) - Structure has collisions.

Physical Measurement Section

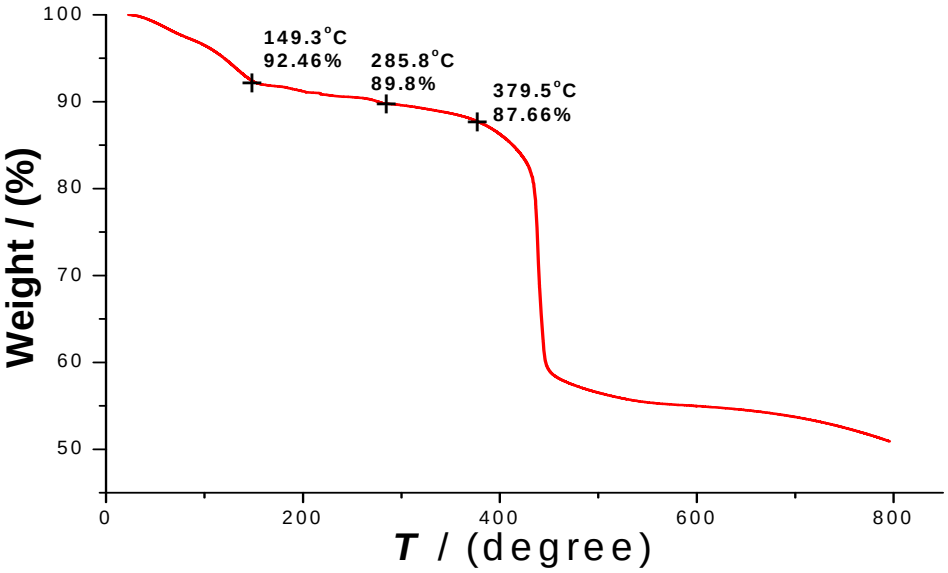

Fig. S4. TG analysis curves of **1**·H_2O·CH_3CH_2OH. The mass loss of ca. 7.54 % at 149.3 °C is related to the loss of guest ethanol solvates (calculated value 7.33 %) in the channels, while the second mass loss of 2.7 % at 285.8 °C is related to the loss of guest water solvates (calculated value 2.86 %), and the third mass loss beginning at 379.5 °C is associated with the decomposition of the host framework.

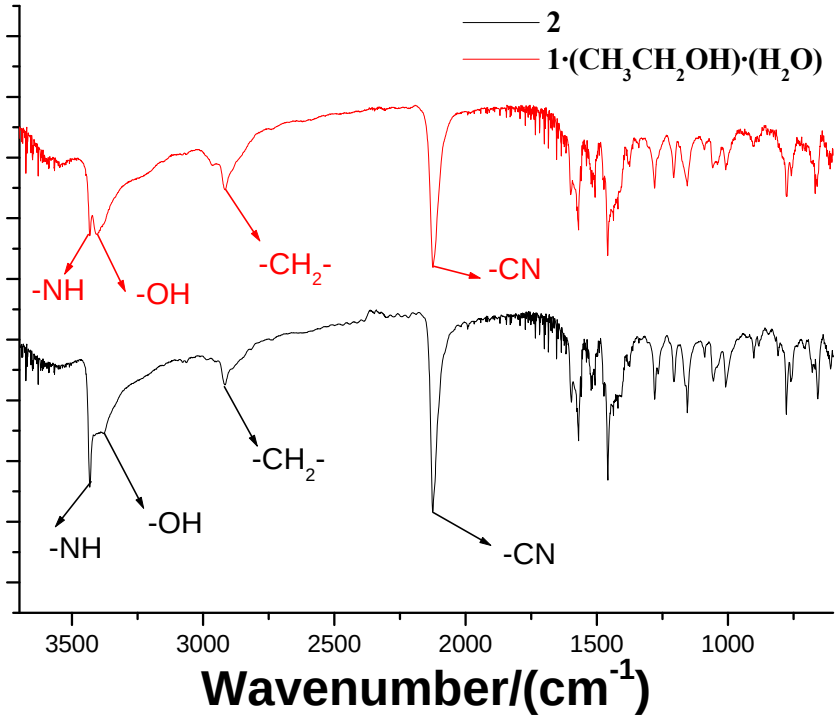

Fig. S5. IR spectra of as-synthesized samples **1**·H_2O·CH_3CH_2OH and desolvated samples **2**. It is shown that the intensity ratio of –OH, –CH_2– to –NH significantly decreased for **2** compared with that of as-synthesized samples **1**·H_2O·CH_3CH_2OH, suggesting the loss of the ethanol and water guests.

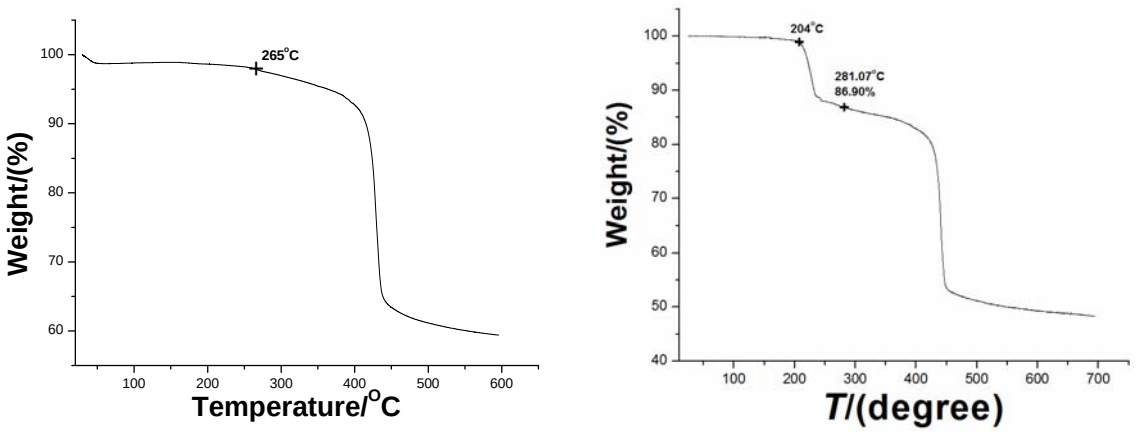

(a) (b)

Fig. S6. (a) TG analysis of desolvated samples **2**. It is shown that the guest molecules in **1**·H_2O·CH_3CH_2OH are largely expelled (the host framework is activated). The mass loss beginning at about 265 °C may be related to the loss of residual H_2O guest and subsequent decomposition of the host framework. (b) TG analysis of **1**·C_6H_{12}.

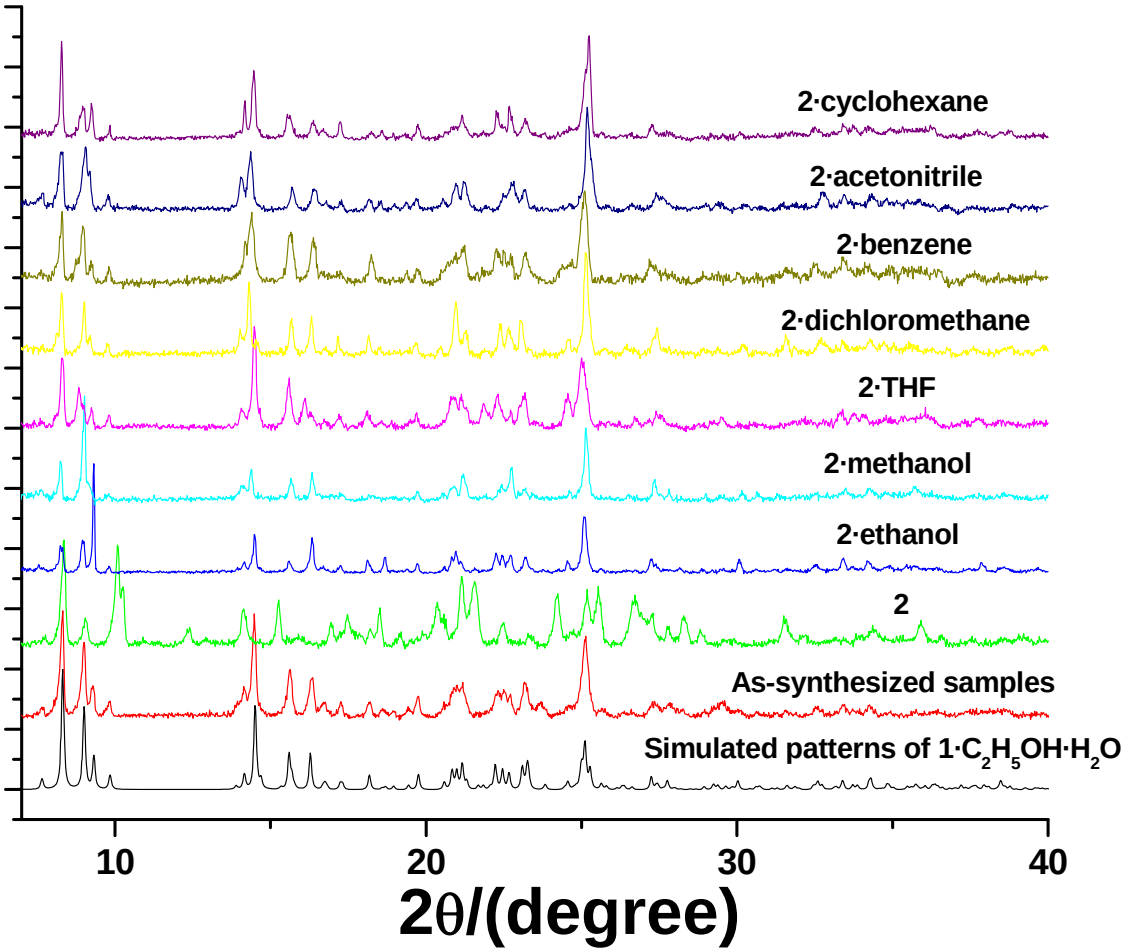

Fig. S7. PXRD patterns of as-synthesized samples **1**·H_2O·CH_3CH_2OH, desolvated samples **2** and **2**·solvents. Note **2**·solvents refer to the products after the solid-liquid sensing procedures by using the activated samples **2** as starting materials. All data were measured at room temperature (298 K).

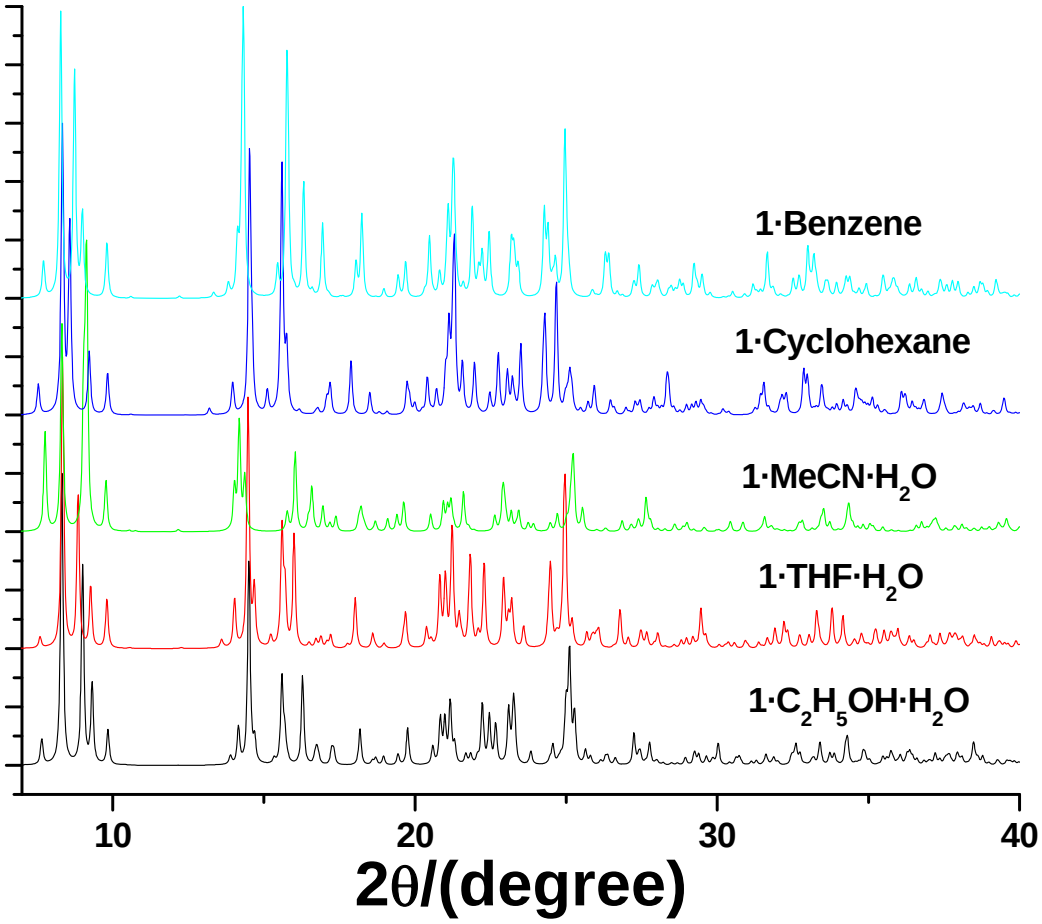

Fig. S8. Comparison of the simulated PXRD patterns (298 K) of **1**·C_6H_6, **1**·THF·H_2O, **1**·H_2O·CH_3CH_2OH, **1**·MeCN·H_2O and **1**·C_6H_{12}.

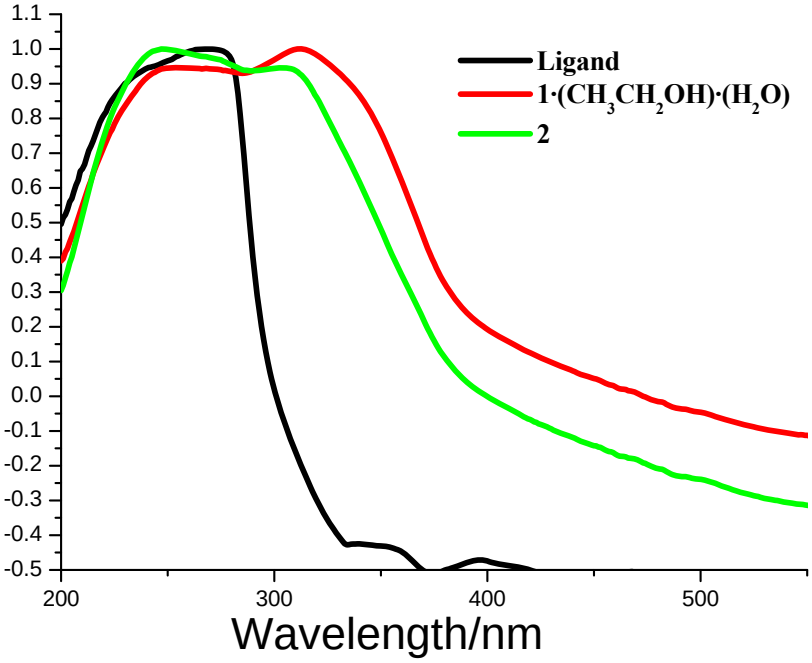

Fig. S9. UV-vis spectra of **1**·H_2O·CH_3CH_2OH, **2** and the ligand in the solid states.

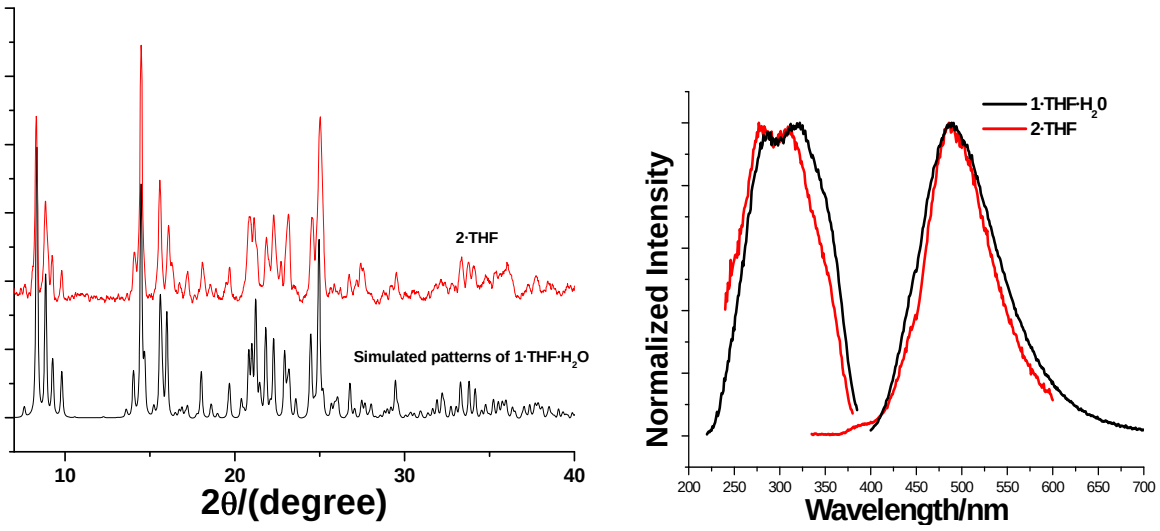

(top)

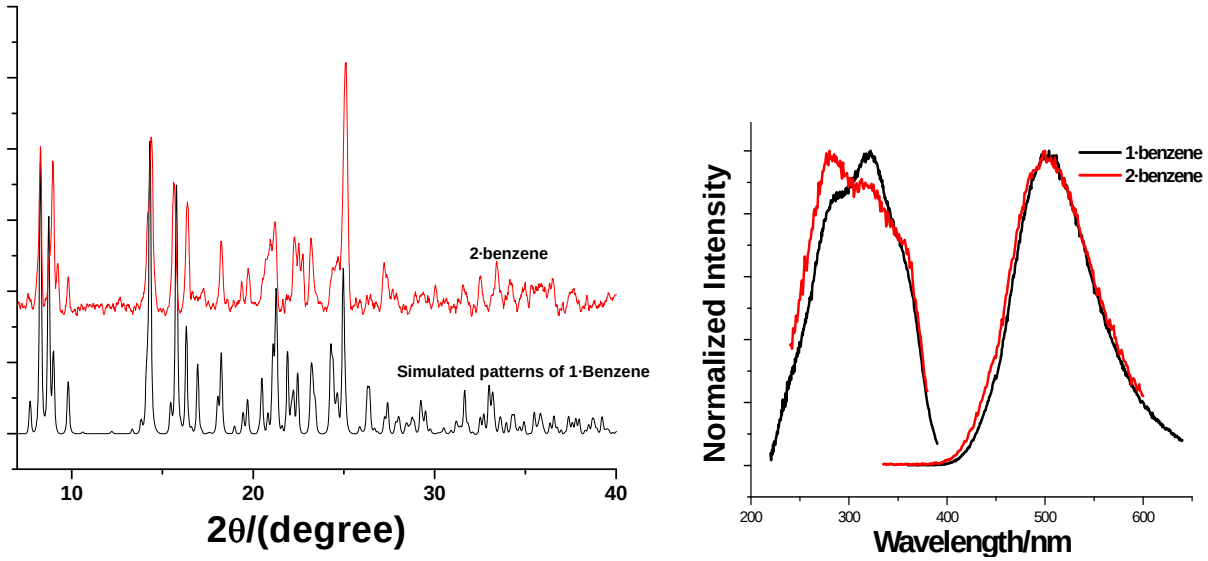

(down)

Fig. S10. Comparison of PXRD patterns and luminescent properties: **1**·THF·H_2O and **2**·THF (top); **1**·benzene and **2**·benzene (down).

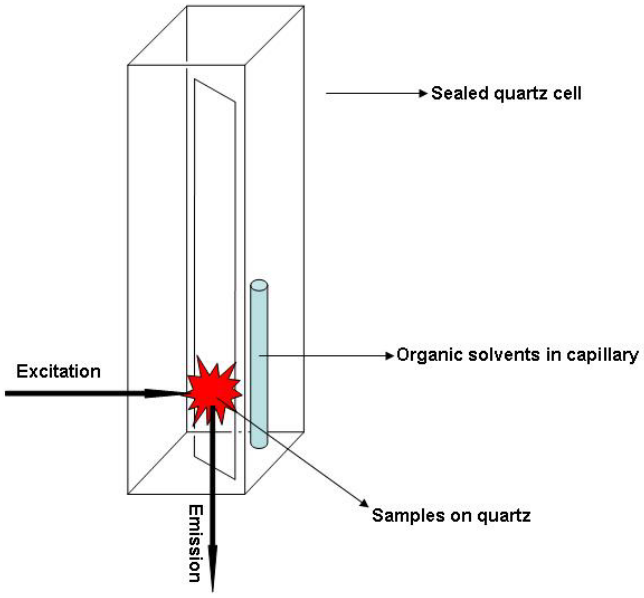

Fig. S11 Experimental setup for the solid-gas detection of acetonitrile vapour.

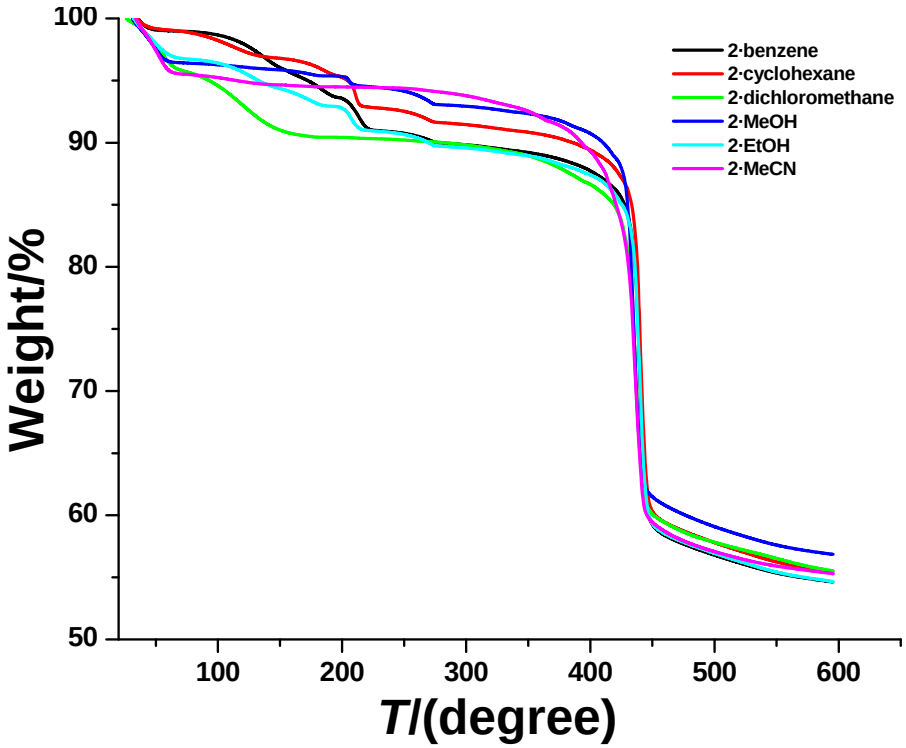

Fig. S12. TG analysis of **2**·solvents

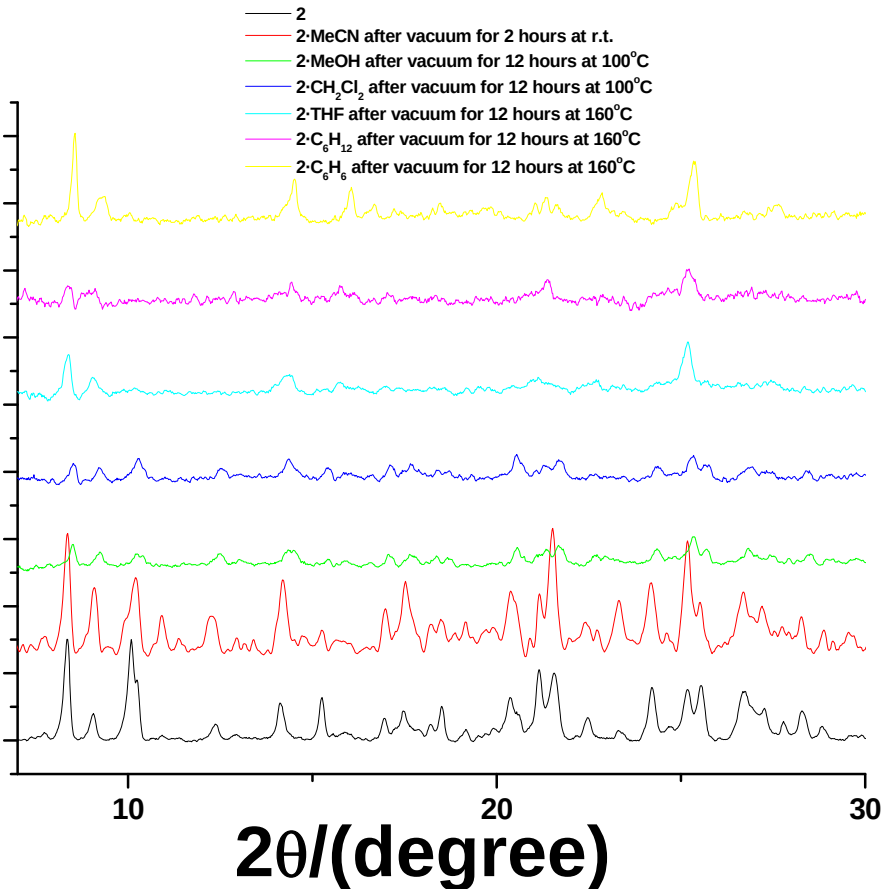

(a)

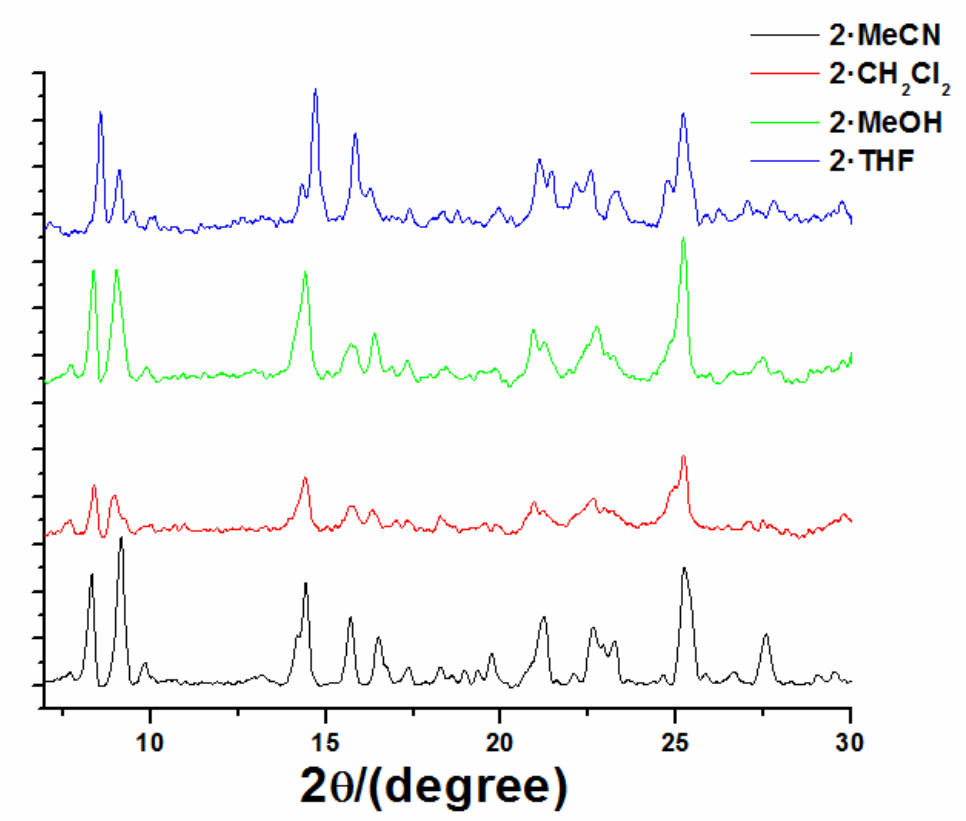

(b)

Fig. S13. (a) Comparison of PXRD patterns of **2**·solvents after evacuation. (b) Comparison of PXRD patterns of reactivated **2** after evacuation after re-immersing into corresponding solvents.

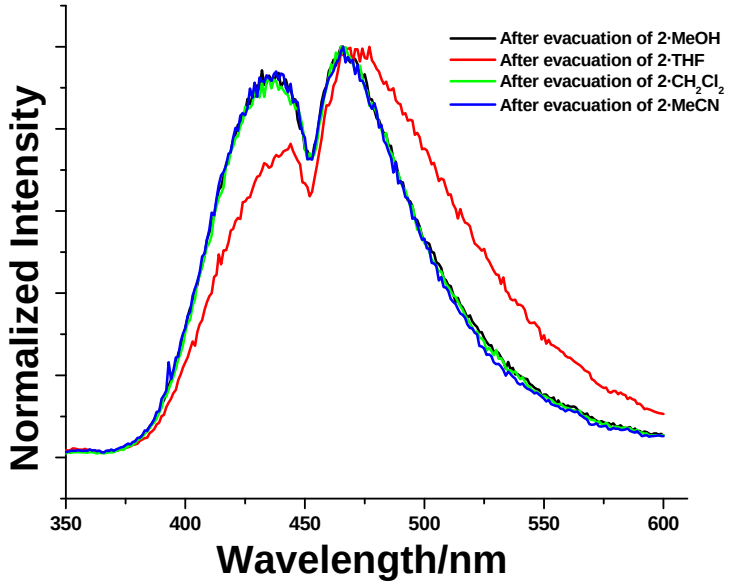

Fig.S14 Solid-state emission spectrum (ex: 320nm) of **2**·solvents after evacuation

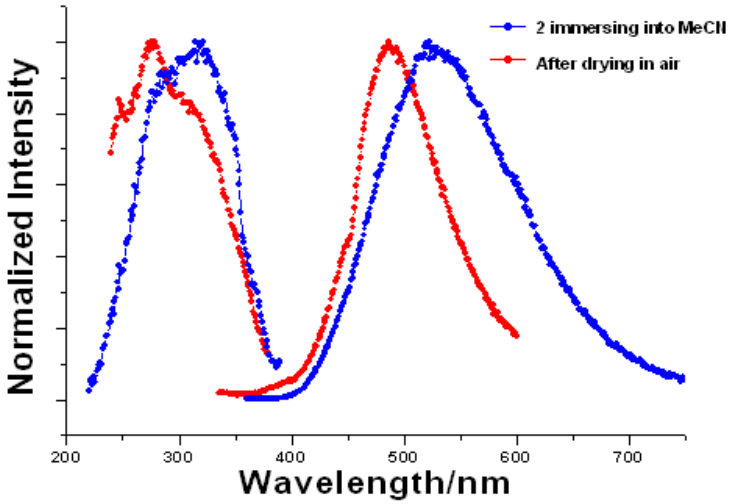

Fig. S15. Excitation and emission changes of **2** immersing into acetonitrile solvent and then drying in air.

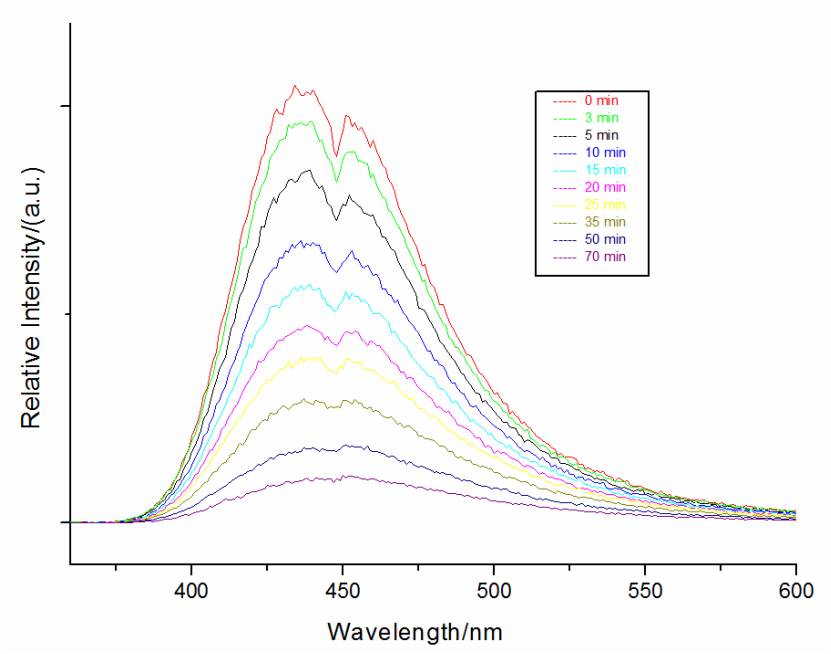

(a)

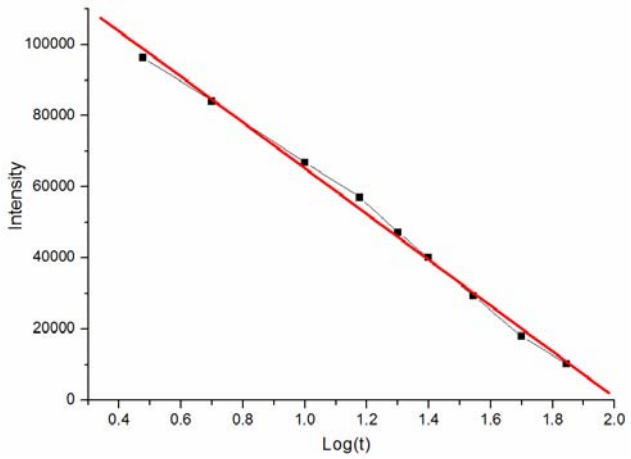

(b)

Fig. S16. (a) Real-time solid-gas sensing of nitrobenzene vapour. (b) The linear relationship between emission intensity and Log(t/sec).